Full Paper

NUMERICAL STUDY ON AIR-CORE VORTEX INSIDE DRAINING TANK USING DIFFERENT COMPUTATIONAL MODELLING APPROACHES

Fadhilah Mohd Sakri[a]*, Mohamed Sukri Mat Ali[b], Sheikh Ahmad Zaki Shaikh Salim[b], Mohd Amzar Azizan[a]

[a]Universiti Kuala Lumpur – Malaysia Institute of Aviation Technology, Jalan Jenderam Hulu, 43800 Dengkil, Selangor, Malaysia
[b]Wind Engineering Laboratory, Malaysia-Japan International Institute of Technology, UTM Kuala Lumpur, 54100 Kuala Lumpur, Malaysia

Graphical abstract

Axially Rotating Vortex

Taylor Vortex Rings
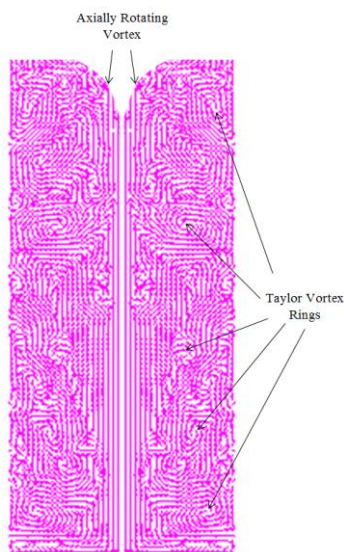
Abstract

Accurate numerical simulation of liquid draining is important to study the physics fluid flow. However, liquid draining involves multiphase and rotational flows, where numerical simulation is expensive to accurately recreate these flow behaviors. The accuracy of numerical results has been also debatable and it is mainly affected by the computational modeling approaches. Therefore, this study evaluates different computational modelling approaches such as DNS, RANS k-ε, RANS k-ω and LES turbulence models. The results for the draining time and flow visualization of the generation of an air-core are in a good agreement with the available published data. The Direct Numerical Simulation (DNS) seems most reasonably satisfactory for VOF studies relating air-core compared to other different turbulence modeling approaches.

Keywords: Air-core, draining tank, turbulence model assessment, OpenFOAM

Abstrak

Simulasi berangka yang tepat untuk penyaliran cecair adalah penting untuk mengkaji aliran bendalir fizik. Walau bagaimanapun, penyaliran cecair melibatkan aliran berlainan fasa dan putaran, di mana simulasi berangka adalah mahal untuk mencipta semula perilaku aliran dengan tepat. Ketepatan keputusan berangka ini juga telah dibahaskan dan sebahagian besarnya dipengaruhi oleh pendekatan pemodelan komputasi. Oleh itu, kajian ini dilakukan untuk menilai pendekatan pemodelan komputasi yang berlainan seperti model DNS, RANS k-ε, RANS k-ω dan model pergolakan LES. Keputusan untuk masa pengaliran dan visualisasi aliran penjanaan teras udara menunjukkan tahap persetujuan yang baik dengan data yang telah diterbitkan. Keputusan dari ujian Simulasi Numerik Langsung (DNS) juga menunjukkan tahap kerkesanan paling memuaskan untuk kajian VOF yang berkaitan dengan teras udara berbanding pendekatan pemodelan turbulensi yang lain.

Kata kunci: Teras udara, tangki penyaliran, penilaian model turbulensi, OpenFOAM.

1.0 INTRODUCTION

The use of Computational Fluid Dynamics (CFD) to predict and understand the dynamics of the liquid draining inside the tank has been well-established in the last thirty years [1]. One of the main advantages of using numerical method is the ability to model the geometry of the system with a wider range of scale and complexity [2], [3]. With the advanced progress in numerical solutions, the introduction of new higher order discretization schemes, accurate predictions can be obtained from the numerical method with less cost compared to the experimental work [4]. Additionally, CFD has the capabilities to provide detailed information of the liquid flow structures and their behaviors.

In this study, a validation and verification study is performed using OpenFOAM (Open Field Operation and Manipulation) [5]. OpenFOAM is an open source CFD-toolbox software for various fluid flow processes [6], [7]. There are many published studies that prove OpenFOAM's capabilities in simulating various flow problems such as computational heat transfer, fluid structure interaction, multiphase and high speed flow. However, only a limited number of studies are focused in the fields of the formation of an air-core vortex inside a draining tank [8], [9]. Therefore, the numerical simulation of a draining tank poses a challenge in the sense that it involves multiphase and rotational flows, where an extended computational period is required.

Most draining tanks exhibit one similar problem which is the formation of an air-core vortex. This problem can be observed during the draining process inside a cylindrical tank. Air-core vortex is one of the rotational motions of the liquid with air entering the vortex through its core [10]. Air-core vortex formation occurs when a dip is formed on the top surface of the liquid as the liquid level reaches a certain critical height, Hc [11]. Then, the dip deepens as the draining process continues and the shape of the liquid surface becomes a long slender string. When the dip reaches the outlet of the tank, this is called air-core vortex [12]. This air-core vortex formation is escalated by the intensification of rotational flow during the draining process [11]. When the core of the vortex reaches the bottom of the tank, the rate of liquid draining is decreased and the flow at the outlet nozzle is unsteady and highly rotational. The air-core vortex, if not properly controlled, can cause vibrations that will reduce the life and efficiency of the storage tank [10].

The formation of air-core vortex involves a complex process. Thus, to accurately recreate the formation of air-core vortex in the numerical simulation, an appropriate treatment of the numerical setting is highly required [13]. Selecting the right turbulence model is also important in order to reproduce the generation of air-core vortex. However, referring to Sohn Chang Hyun *et al*. [14], Park and Sohn [15], Jong Hyeon Son *et al*. [16] and Madsen *et al*. [17], the DNS is still the best solution to accurately recreate the formation of air-core vortex. The main objective of this paper is to evaluate different computational modelling approaches (DNS, RANS $k-\varepsilon$, RANS $k-\omega$ and LES turbulence models). The axi-symmetric boundary condition (wedge) and the turbulence model which have been applied in this research are further explained in detailed in the paper. Additionally, this study also revisits the fundamental physics flow of the generation of an air-core vortex. Comparisons between the simulation result with the previously published data by Park and Sohn [15] and Jong Hyeon Son *et al*. [16] are also discussed to validate the capability of the axi-symmetric boundary condition and the numerical settings in simulating the liquid draining inside a tank.

2.0 METHODOLOGY

A cylindrical tank of diameter *(D)* 90mm and length *(L)* of 450mm is partially filled with water. The initial height of the water measured from the bottom of the tank (h_o) is 350mm. A drain nozzle is located at the centre of the tank's bottom surface. The drain nozzle's diameter *(d)* is 6mm whereas its length *(l)* is 15mm. The top and bottom surfaces of the tank is open, i.e., in atmospheric condition. The fluid is drained downward naturally by gravity, g. This geometry is intentionally made the same as the experimental and numerical investigations of Park and Sohn [15] for direct comparisons to the study. Figure 1 shows the schematic diagram of the problem geometry.
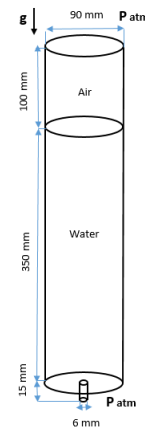

Figure 1 Schematic diagram of the draining tank

In this study, two flow conditions are being simulated. The first condition is for the non-swirl cases where the liquid is drained from the stagnant condition. Comparisons between the full geometry (3D) and axi-symmetric boundary condition are discussed. The second condition involves swirl cases where the liquid is initially rotated at the speed of 120 RPM before being drained out by gravity. Experimental and numerical comparisons between the previously published studies by Park and Sohn [15] are discussed. Additionally, this paper also discusses the intermittent phenomenon of reverse jet during the generation of air-core vortex.

2.1 Governing Equations

The conservation equations for mass and momentum for incompressible, transient and free surface flows are given as follow [5], [12], [18], [19].

$$\nabla.U = 0 \tag{1}$$

$$\frac{\partial \rho U}{\partial t} + \nabla.\rho UU - \nabla.(\rho\Gamma_U\nabla_U) = S_U(U) + g + F \tag{2}$$

Here, U is the local velocity at instantaneous time, ρ is the density, and Γ is the diffusion coefficient. A transformation from PDE to the linearized algebraic equation needs to be completed prior to solving the equations that describe the flow transport. Equation (2) above shows the standard form of the transport equation.

All terms in equation (2) are integrated over time ranging from $t \rightarrow t + \Delta t$ with the control volume V_p [5]:

$$\int_t^{t+\Delta t} \left[\frac{\partial}{\partial t} \int_{V_p} \rho dV + \int_{V_p} \nabla.(\rho UU)dV - \int_{V_p} \nabla.(\rho\Gamma_U\nabla U) \right] dt = \int_t^{t+\Delta t} \left[\int_{V_p} S(U)dV \right] dt \tag{3}$$

where S is all source terms and index p describes the midpoint of the control volume. In the left side, the first part represents the temporal term, the second term defines the convective transport, the third term illustrates the diffusive transport and the right side represents sources. Table 1 and Table 2 describe the numerical schemes for non-swirl cases and swirl cases, respectively.

2.2 Multiphase Solvers

In this study, the 'interFoam' solver is used. Herein, only one momentum and one mass conservation equation are determined for both fluids. Thus, viscosity and density of both fluids are averaged based on the volume fractions in the cell [20].

Volume of Fluid (VOF) is adopted to track the shape and position of the interface by solving an equation for the volume fraction of each cell [20]. The method requires a minimum storage as it follows regions rather than surfaces.

In the Volume of Fluid (VOF) method, α is a function that indicates the relative fraction between liquid and gas in each cell of the physical domain. $\alpha = 0$ is when the fluid is in the gas phase and $\alpha = 1$ is when the fluid is in the liquid phase. Meanwhile, a liquid-gas interface presence in the cell is between 0 and 1. The volume fractions of all phases in a cell sum to unity. Hence, the following equation must be fulfilled:

$$\alpha_g + \alpha_l = 1 \tag{4}$$

where α_l and α_g are the volume fractions of liquid and gas, respectively.

In order to obtain a spatial distribution of the volume fraction, the governing equation set for the basic flows in equations (1) and (2) should be solved together with the following conservation equation for one single phase:

$$\frac{\partial}{\partial t}(\rho\alpha_l) + \frac{\partial}{\partial x_i}(\rho u_i\alpha_l) = 0 \tag{5}$$

Equation (5) describes the balance between the transient change of the volume fractions in a cell and its flux through the interfaces of the cell. The dynamic viscosity and density of each cell are determined as shown below:

$$\rho = \alpha_l\rho_l + \alpha_g\rho_g$$
$$\mu = \alpha_l\mu_l + \alpha_g\mu_g \tag{6}$$

Table 1 Order of accuracy and the numerical scheme of each differential operator in non-swirl cases [4]

Term	Scheme	Order of convergence	Interpolation scheme
$\frac{\partial}{\partial t}, \frac{\partial^2}{\partial^2 t}$	Euler	$O(h)$	
∇	Gauss	$O(h^2)$	Linear
$\nabla.(\rho\phi, U)$	Gauss	$O(h^2)$	Linear
$\nabla.(\phi, \alpha)$	Gauss	$O(h^2)$	vanLeer
$\nabla.(\phi, k)$	Gauss	$O(h)$	upwind
$\nabla.(\phi, \varepsilon)$	Gauss	$O(h)$	upwind
∇^2	Gauss	$O(h^2)$	linear corrected

Table 2 Order of accuracy and numerical scheme of each differential operator in swirl cases [4]

Term	Scheme	Order of convergence	Interpolation scheme
$\frac{\partial}{\partial t}, \frac{\partial^2}{\partial^2 t}$	Euler	$O(h)$	
∇	Gauss	$O(h^2)$	vanLeer
$\nabla.(\rho\phi, U)$	Gauss	$O(h^2)$	Linear
$\nabla.(\phi, \alpha)$	Gauss	$O(h^2)$	vanLeer

Term	Scheme	Order of convergence	Interpolation scheme
$\nabla.(\phi, k)$	Gauss	$O(h)$	upwind
$\nabla.(\phi, \varepsilon)$	Gauss	$O(h)$	upwind
∇^2	Gauss	$O(h^2)$	linear corrected

Here, the surface tension force is calculated as follows:

$$F = \sigma \frac{\rho k \nabla \alpha_l}{0.5(\rho_l + \rho_g)} \qquad (7)$$

$$k = -\nabla.\left(\frac{\nabla \alpha_l}{|\nabla \alpha_l|}\right) \qquad (8)$$

Where, k is the curvature and σ is the surface tension.

2.3 Boundary Conditions

According to Jasak [5], boundary conditions set down the series of faces in the computational mesh which correspond to the boundaries of the physical domain. They are separated into numerical and physical boundary conditions. Numerical boundary conditions have two standard types: Dirichlet (fixed) boundary condition to determine the value of the variable on the boundary, and Von Neumann boundary condition to define the gradient of the variable normal to the boundary. Meanwhile, physical boundary conditions are walls, symmetry planes, outlet, inlet etc. The physical boundary conditions for the incompressible flow that have been adopted for this study are explained and listed in Table 3. The boundary conditions that have been employed are listed in Tables 4, 5 and 6.

2.4 Axi-symmetric Boundary Condition (wedge)

An axi-symmetric boundary condition is named as 'wedge' in OpenFOAM. This boundary condition is applied to two-dimensional axi-symmetric cases specifically for a cylindrical geometry. Since the tank with the cylinder geometry is adopted, the axi-symmetric boundary condition is reliable and applicable to this study. Figure 2 displays the configurations of axi-symmetric boundary condition in OpenFOAM. The figure shows a wedge with a small angle (<5⁰) and 1 thick cell running along the plane of symmetry. This plane has been set as different patches of wedge types such as wedge patch 1 and wedge patch 2 [21].
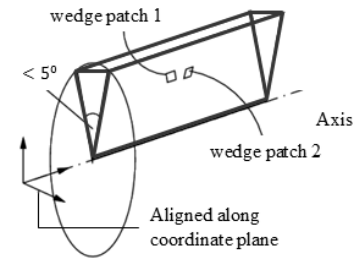

Figure 2 Axi-symmetric boundary condition in OpenFOAM [21]

Table 3 Explanation of physical boundary conditions

Type	Description of boundary conditions
zeroGradient	Normal gradient of ϕ is zero
fixedValue	Value of ϕ is specified
pressureInletOutletVelocity	Combination of *pressureInletOutletVelocity* and *inletOutlet* (pressureInletVelocity: When P is known at inlet, U is evaluated from the flux, normal to patch)
totalPressure	Total pressure $\mathcal{P}_0 = \mathcal{P} + \frac{1}{2}\rho|U|^2$ is fixed; when U changes, $\mathcal{P}$ is adjusted accordingly
inletOutlet	Switches U and between *fixedValue* and *zeroGradient* depending on direction of U
bouyantPressure	Sets fixedGradient pressure based on the atmospheric pressure gradient
calculated	Boundary field ϕ derived from other fields
rotatingWallVelocity	Determines the velocity at the surface of a rotating body
nutkWallfunction	On corresponding patches in the turbulent fields k and nut.
kqRWallFunction	On corresponding patches in the turbulent fields k, q and R
wedge	Wedge front and back for an axisymmetric geometry

Table 4 Boundary conditions for the non-swirl case

BC	Type of Patches		
	Outlet	Inlet	Walls
a	zeroGradient	inletOutlet	zeroGradient
U	zeroGradient	pressureInletOutletVelocity	fixedValue
ρ rgh	fixedValue	totalPressure	bouyantPressure
k	zeroGradient	inletOutlet	kqRWallFunction

BC	Type of Patches		
	Outlet	**Inlet**	**Walls**
nuT	*calculated*	*calculated*	*nutkWallfunction*
nuTilda	*zeroGradient*	*inletOutlet*	*zeroGradient*

Table 5 Boundary conditions for the swirl case (rotating tank)

BC	Type of Patches		
	Outlet	Inlet	Walls
a	*zeroGradient*	*inletOutlet*	*zeroGradient*
U	*rotatingWallVelocity*	*pressureInletOutletVelocity*	*fixedValue*
ρ rgh	*bouyantPressure*	*totalPressure*	*bouyantPressure*
k	*kqRWallFunction*	*inletOutlet*	*kqRWallFunction*
nuT	*nutkWallfunction*	*calculated*	*nutkWallfunction*
nuTilda	*zeroGradient*	*inletOutlet*	*zeroGradient*

Table 6 Boundary conditions for the swirl case (draining)

BC	Type of Patches		
	Outlet	Inlet	Walls
a	*fixedValue*	*fixedValue*	*zeroGradient*
U	*zeroGradient*	*zeroGradient*	*fixedValue*
ρ rgh	*fixedValue*	*fixedValue*	*bouyantPressure*
k	*zeroGradient*	*inletOutlet*	*kqRWallFunction*
nuT	*calculated*	*calculated*	*nutkWallfunction*
nuTilda	*zeroGradient*	*inletOutlet*	*zeroGradient*

3.0 RESULTS AND DISCUSSIONS

3.1 Comparison of Drainage Time

Three turbulence model ($k − \varepsilon$, $k − \omega$ and LES) are assessed in addition to the Direct Numerical Simulation (DNS). The sensitivity of the results of the time discretization scheme is also assessed for all turbulence models. Table 7 compares the result of the current study with the similar study by Park and Sohn [22]. The theoretical value that is calculated from equation (9) is also compared.

$$t = \frac{\sqrt{h_0} − \sqrt{h}}{\sqrt{\frac{g}{2}}} \left(\frac{d_t}{d_n} \right)^2 \qquad (9)$$

In the case of 1st order of time discretization scheme, the draining time completion obtained from the current simulation using DNS, RANS $k − \varepsilon$, RANS $k − \omega$ and LES are 91s, 72s, 70s and 101.5, respectively. The draining times for RANS $k − \varepsilon$ and RANS $k − \omega$ are 8.26s and 10.26s earlier than the result obtained from the experiment by Park and Sohn [23]. Meanwhile, the draining time completion obtained from DNS and LES are 10.74s and 21.24s slower than the result obtained from the experiment by Park and Sohn [23]. Not much change are observed when the time discretization is changed to 2nd order scheme.

Table 7 The comparison of draining time of the swirl case between published data by Park and Sohn (experimental, theoretical and numerical), and current studies (DNS, RANS $k − \varepsilon$ and RANS $k − \omega$)

Case	1st order t_{drain} [s]	2nd order t_{drain} [s]
Park & C.H Sohn (Exp.)	80.26	-
Park & C.H Sohn(Num.)	82.32	-
Theoretical	83.48	-
Current simulation (DNS)	91	90
Current simulation (RANS $\boldsymbol{k − \varepsilon}$)	72	70
Current simulation (RANS $\boldsymbol{k − \omega}$)	70	68.5
Current simulation (LES)	101.5	100

3.2 Flow Visualization of Air-core Formation

Figures 3-6 show the progression of liquid draining obtained from DNS, RANS $k − \varepsilon$, RANS $k − \omega$ and LES, respectively. At the beginning of the draining process (t=0), the top surface of the liquid is in parabolic shape. This is due to the centripetal force from the initial wall rotation and the density difference

between liquid and air. The parabolic shape for RANS $k - \varepsilon$ and RANS $k - \omega$ are more obvious than DNS and LES due to the Reynolds stress term from the convective acceleration which effects on the mean flow [24]. However, at time 15s of draining process, the top surface of the liquid is flat for the case RANS $k - \varepsilon$ and RANS $k - \omega$. The shape remains the same until the end of the draining process. A different shape is observed for DNS and LES where a dip is observed near the centre of the tank. As the draining process continues, the dip extends till the outlet of the tank (happens at t=21s) at which the air-core generation is fully completed. At this moment, the dip raises into a vortex with an air-core and the free surface creates a long and slender string shape lengthens to the bottom of the tank, and it is named as air-core vortex [14]. As the level reaches a certain critical height Hc, the dip forms into the air-core on the surface which consequently enters the outlet [11]. This phenomenon repetitively continued until the draining finished (except when the reverse jet is occurred). The flow at the outlet nozzle is highly rotational and the rate of liquid draining is decreased when the core of the vortex extents to the bottom of the tank [13].
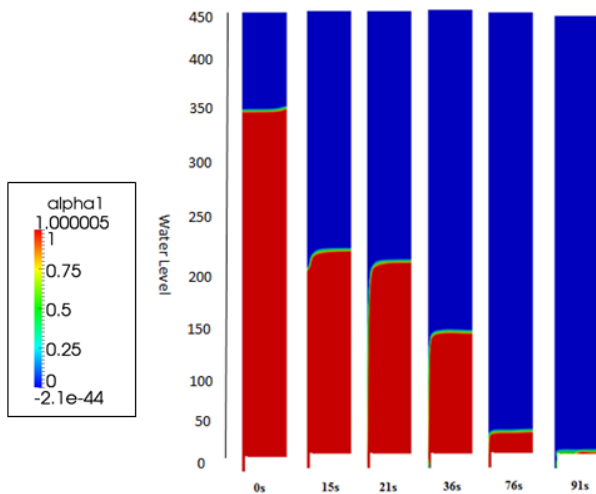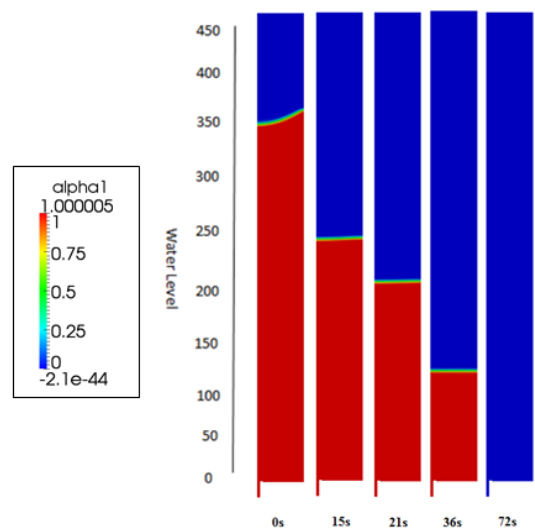

Figure 4 No generation of the air-core for the current simulation (RANS $k - \varepsilon$) at drain time 0-72s (1st order of discretization scheme)
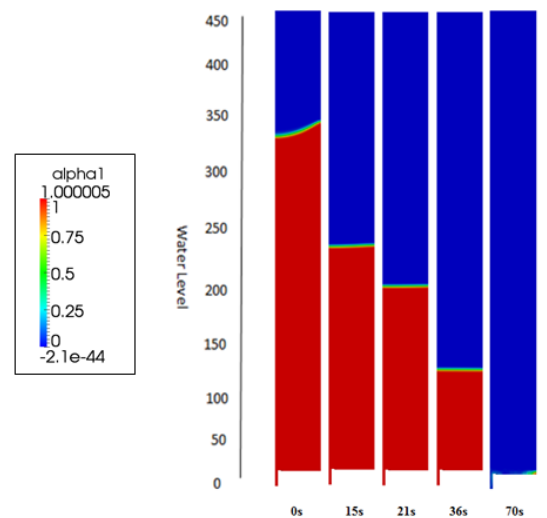

Figure 3 Generation of the air-core for the current simulation (DNS) at drain time 0-91s (1st order of discretization scheme)

Figure 5 No generation of the air-core for the current simulation (RANS $k - \omega$) at drain time 0-70s (1st order of discretization scheme)
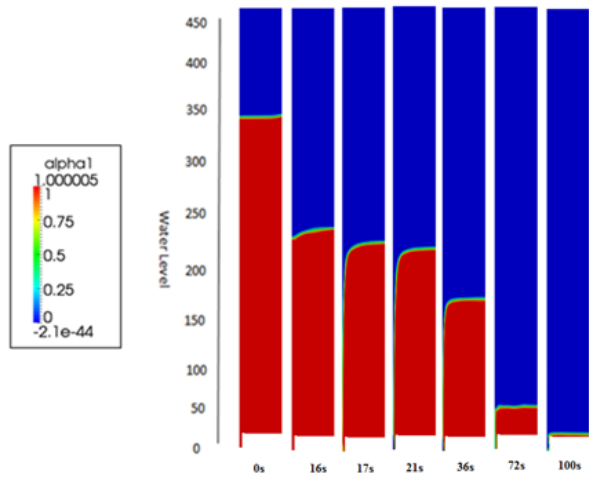
Figure 6 Generation of the air-core for the current simulation (LES) at drain time 0-100s (2nd order of discretization scheme)

Figure 7 Close-up velocity vector distribution for the current simulation (DNS) at drain time 21s

3.3 Velocity Vector Inside the Tank Ow Visualization of Air-core Formation

Figure 7-10 show the velocity vector distributions at drain time 21s ($h = 200mm$) for the DNS, RANS $k - \varepsilon$, RANS $k - \omega$ and LES, respectively. In Figure 7 and 10, an axial flow and numbers of multi-vortex structures rotating with circumferential axis are observed inside the tank. Referring to Jong Hyeon Son *et al*. [25], this combination of flow structures is known as toroidal vortex (see Figure 11). The multi-vortex structures are called as Taylor vortices. These vortices are stimulated by two angular velocities which are inner and outer regions in the tank. As shown in Figure 7 and 10, the blue arrow with a clockwise direction signifies positive values of angular velocity and the red arrow with a counter clockwise direction symbolizes negative values of the angular velocity. Meanwhile, the axially rotating vortex in the central is formed by the angular momentum conservation since the fluid particles are moved from the side wall to the centre by the draining [25]. According to Jong Hyeon Son *et al*. [25], the liquid in the Taylor vortices cannot be combined with the rotating axially in the centre of the tank since it limits the liquid in the off area. So, at the first, only the liquid in the centre of the tank is drained out. The stack structures of Taylor vortices (see Figure 11) act like a block and makes the condition where a shallow water drain, even though the water level is considerably lower. Thus, the dimple on the free surface is pulled downward and finally, the air-core is reproduced. In the Figure 8 and 9, there are no Taylor vortices have been discovered in order to accelerate the axially rotating vortex to regenerate the air-core. Hence, in the case of RANS $k - \varepsilon$ and RANS $k - \omega$, there are no generation of air-core is observed.
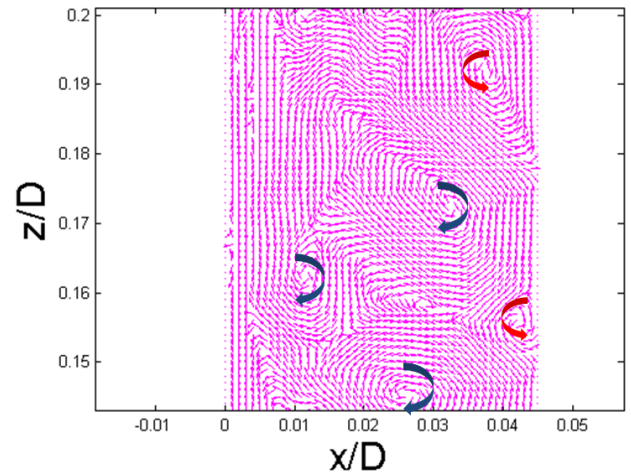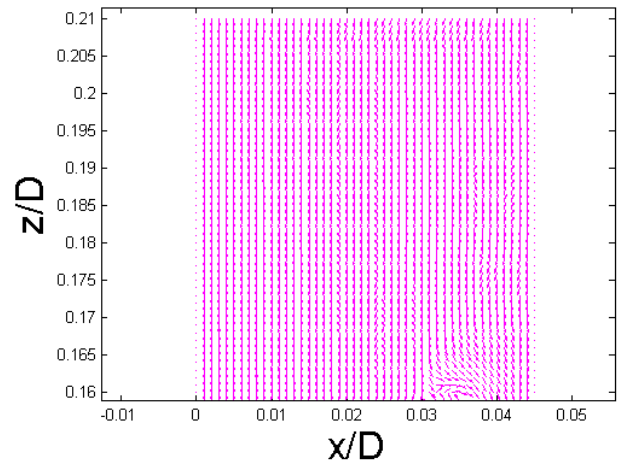

Figure 8 Close-up velocity vector distribution for the current simulation (RANS $k - \varepsilon$) at drain time 21s
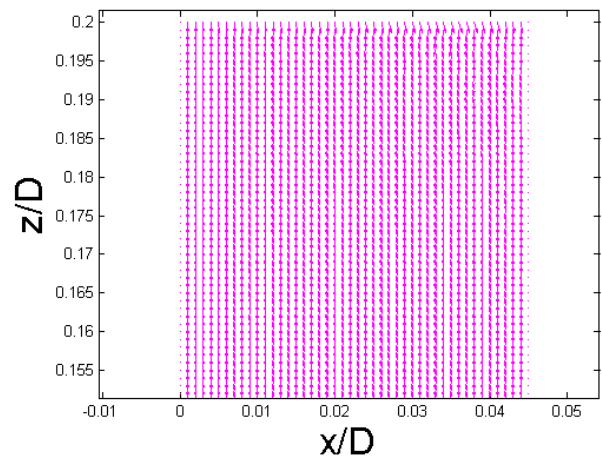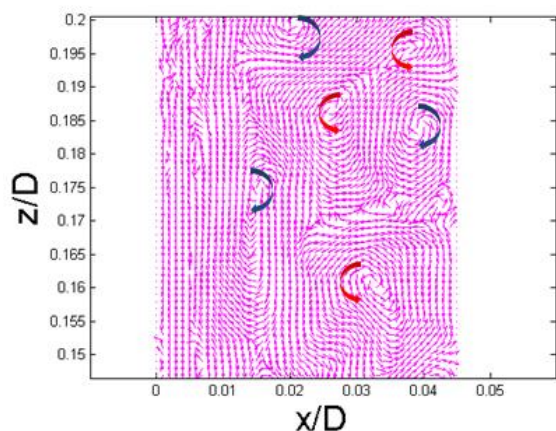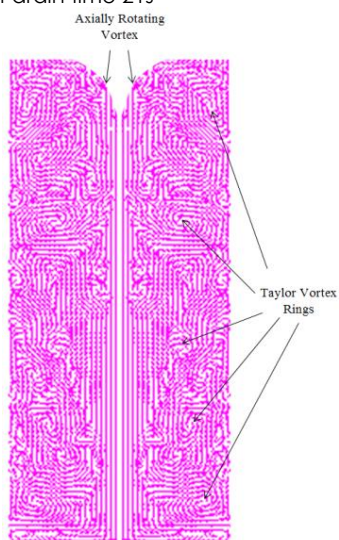

Figure 9 Close-up velocity vector distribution for the current simulation (RANS $k - \omega$) at drain time 21s

Figure 10 Close-up velocity vector distribution for the current simulation (LES) at drain time 21s

Figure 11 Velocity vector distribution of the interaction between the axially rotating vortex and the Taylor vortex rings for the current simulation (DNS) at drain time 21s

4.0 CONCLUSIONS

In this paper, the liquid draining inside the cylindrical tank was successfully investigated through the axi-symmetric (wedge) boundary condition in the OpenFOAM framework. The wedge boundary condition shows an excellent result of simulating the condition. The result also show that the current simulations (DNS, RANS $k - \varepsilon$, RANS $k - \omega$ and LES models) are able to reproduce the liquid draining process inside the tank in all cases. From the comparison of drain time plots, the current DNS demonstrates a very similar pattern and value with the result obtained from the experimental measurement of Park and Sohn (2011). The ellipsoidal shape of the free surface was also successfully recreated in all cases at the beginning of the liquid draining. In the DNS and LES cases, the finer grid is also successfully reproduced the generation of air-core and it is in a good agreement with the result of Jong Hyeon Son *et al.* (2015). However, based on the results from the

second stage, DNS is most reasonably satisfactory for VOF studies relating air-core compared to other different modelling approaches.

References

[1]   B. T. Lubin and G. S. Springer. 1967. Formation of A Dip on The Surface of A Liquid Draining From A Tank. *Journal of Fluid Mechanics*. 29: 385-390.
[2]   EPRI. 2014. High Performance Computing in the Electric Power Industry," EPRI Technology Insights.
[3]   2013. Use of Computational Fluid Dynamics Codes For Safety Analysis of Nuclear Reactor Systems. IAEA-TECDOC-1379.
[4]   L. M. Rechiman, M. I. Centero and E. A. Dari. 2014. Hydrodynamic Transient Assessment of a Draining Tank. *Mecanica Compuatational.* Xxxiii: 2927-2938.
[5]   H. Jasak. 1996. Error Analysis and Estimation for the Finite Volume Method with Applications to Fluid Flows. Thesis. London, England: Imperial Collage.
[6]   E. Robertson, V. Choudhury and D. Walters. 2015. Validation of Open FOAM Numerical Methods and Turbulence Models for Incompressible Bluff Body Flows. *Computer and Fluids.* 123(2015): 122-145.
[7]   W. HG, T. G, J. H and F. C. 1998. A Tensorial Approach to Computational Continuum Mechanics Using Object-Oriented Techniques. *Comput Phys.* 12: 620-31.
[8]   K. Ramamurthi and T. John Tharakan. 1995. Intensification of a Vortex during Free Draining. *The Canadian Journal of Chemical Engineering.* 73.
[9]   Mcduffie and N. G. 1977. Vortex Free Downflow in Vertical Drains. *AIChE Journal.* 23: 1.
[10] Fadhilah, M. S., Mohamed Sukri, M. A., Syeikh Ahmad Zaki S. S. and Sallehuddin Muhamad. 2016. Numerical Simulation of Liquids Draining from a Tank Using Open Foam. CFRI, Kuala Lumpur.
[11] Prateep Basu, Dheraaj Agarwal, T. John Tharakan and A. Salih. 2013. Numerical Studies on Air-core Vortex Formation during Draining of Liquids from Tanks. *International Journal of Fluid Mechanics Research*. 40(1): 27-41.
[12] Sohn Chang Hyun, Son Jong Hyeon and Park II Seouk. 2012. Numerical Analysis of Vortex Core Phenomenon During Draining from Cylinder Tank for Various Initial Swirling Speeds and Various Tank and Drain Port Sizes. *Journal of Hydrodynamics.* 25(2): 183-195.
[13] F. Mohd Sakri, M. S. Mat Ali, S. A. Z. Shaikh Salim. 2016. Computational Investigations and Grid Refinement Study of 3D Transient Flow in a Cylindrical Tank Using Open FOAM. AEROTECH, Kuala Lumpur.
[14] Sohn Chang Hyun, Son Jong Hyeon and Park II Seouk. 2013. Numerical Analysis of Vortex Core Phenomenon during Draining from Cylinder Tank for Various Initial Swirling Speeds and Various Tank and Drain Port Sizes. *Journal of Hydrodynamics.* 25(2): 183-195.
[15] II Seouk Park and Chang Hyun Sohn. 2011. Experimental and Numerical Study on Air Cores for Cylindrical Tank

Draining. *International Communications in Heat and Mass Transfer*. 38: 1044-1049.

[16]   J. H. Son, C. H. Sohn and I. S. Park. 2015. Numerical Study of 3D air-core Phenomenon during Liquid Draining. *Journal of Mechanical Science and Technology*. 29: 10.

[17]   J. Madsen, B. H. Hjertager and T. Solberg. 2004. Numerical Simulation of Internal Flow in a Large-Scale Pressure-Swirl Atomizer. ILASSS-Europe (Denmark).

[18]   H. K. Versteeg and W. Malalasekera. 2008. *An Introduction to Computational Dynamics-The Finite Volume Method*. 2nd edition. New York: Pearson Education Ltd.

[19]   R. Aris, Vector. 1989. *Tensors and the Basic Equations of Fluid Mechanics.* Dover Publications,

[20]   L. Shulze and C. Thorenz. 2014. The Multhiphase Capabilitis of the CFD Toolbox OpenFOAM for Hydraulic Engineering Applications. ICHE 2014, Hamburg.

[21]   C. J. Greenshields. 2015. Open FOAM User Guide 2015. [Online].

[22]   Il SeoukPark and Chang Hyun Sohn. 2011. Experimental and Numerical Study on Air Cores for Cylindrical Tank Draining.

[23]   Il SeoukPark and Chang Hyun Sohn. 2011. Experimental and Numerical Study on Air Cores for Cylindrical Tank Draining. International Communications in Heat and Mass Transfer. 38: 1044-1049.

[24]   Andersson and Bengt. 2012. Computational Fluid Dynamics for Engineers. Cambridge University Press, Cambridge.

[25]   J. H. Soon, C. H. Sohn and I. S. Park. 2015. Numerical Study of 3D Air-Core Phenomenon during Liquid Draining. *Journal of Mechanical Science and Technology*. 29(10): 4247-4257,